Metamorphosis of ultrathin Ni oxide nanostructures on Ag(100)

W. Steurer,[1] F. Allegretti,[1,*] S. Surnev,[1] G. Barcaro,[2] L. Sementa,[2] F. Negreiros,[2] A. Fortunelli,[2] and F. P. Netzer[1]
[1]*Surface and Interface Physics, Institute of Physics, Karl-Franzens University Graz, A-8010 Graz, Austria*
[2]*CNR-IPCF, Istituto per i Processi Chimico-Fisici del CNR, I-56124 Pisa, Italy*
(Received 29 July 2011; published 26 September 2011)

The evolution of the morphology of Ni-oxide nanostructures on Ag(100) as a function of temperature has been followed experimentally by scanning tunneling microscopy (STM) and theoretically by density-functional theory (DFT) calculations. After reactive deposition at room temperature and annealing at 450 K, the NiO(2×1) phase embedded into the Ag substrate is formed due to kinetic stabilization during growth. The (2×1) structure is replaced by the thermodynamically more stable NiO(100)(1×1) phase, also embedded into the Ag substrate, for annealing at $T > 500$ K. As shown by DFT modeling and in agreement with experimental STM contrast, the formation of second-layer NiO patches below the NiO(1×1) monolayer is an effective means of strain relief in the NiO(1×1) monolayer islands. For $T > 600$ K, the increased possibilities of mass transport lead to an intriguing surface morphology called "labyrinth" phase, with narrow high-aspect ratio embedded NiO(1×1)-type islands. The latter are stabilized by the interaction of the NiO borders with the Ag(100) substrate via double-layer boundary lines, which according to the DFT calculations provide the essential elements of this thermodynamic ground state.

DOI: 10.1103/PhysRevB.84.115446 PACS number(s): 68.47.Gh, 68.37.Ef, 68.35.Rh, 62.23.St

I. INTRODUCTION

The Ni-oxide on a Ag(100) system constitutes a prototypical example of a highly correlated transition-metal oxide coupled to a noble metal surface. The study of thin NiO_x films on a silver support is not only of interest from the viewpoint of their electronic and catalytic properties, but also in view of their magnetic properties and potential applications in magnetic nanodevice technology.[1] Understanding the influence of the morphology and layer thickness on these properties is of particular interest. For example, the ability to control the oxide thickness opens up the opportunity of band-gap engineering with a wide range of important applications.[2] The morphology of the grown films is an important property which has a decisive influence on the presence of island and phase boundaries and defects of various kinds, and thus on the electronic structure of the interface,[3] which in turn determines the energetics of the whole system.[4,5] The morphology of a film is strongly influenced by the early stages of thin-film growth, and for this reason, in this paper we address the morphology and structure of NiO_x nanophases up to one monolayer coverage on a Ag(100) surface.

Previous work has shown that ultrathin films of Ni oxide deposited on Ag(100) by reactive evaporation in an oxygen atmosphere form several-layer-thick islands embedded into the Ag substrate.[6–8] For submonolayer coverages, a NiO $p(2 \times 1)$ precursor phase forms upon deposition. The (2×1) phase is of monoatomic thickness and gradually covers the surface upon increasing the surface coverage.[9] It can be transformed into a NiO(100)(1×1) structure by postannealing at around 500 K. The O/Ni ratio of the $p(2 \times 1)$ and (1×1) phases remains unchanged during this transition;[9] however, an increase of the fraction of the substrate surface not covered by the oxide has been revealed by low-energy ion-scattering (LEIS) experiments[9] and scanning tunneling microscopy (STM) images.[6,7] The influence of the annealing conditions (oxygen partial pressure, temperature) on the morphology of the NiO(100)(1×1) phase has been explored by various groups. Well-defined rectangular island shapes with polar island boundaries (i.e., rows of either Ni or O atoms) have been reported for annealing at 450 K in the absence of O_2.[6,8] In contrast, Caffio *et al.* have observed more roundish island shapes upon annealing at 500 K in vacuum and have ascribed the occurrence of the geometric island shapes to oxygen-rich annealing conditions.[7] In either case, however, the stoichiometry of the film appears to remain the same. Recently, Rota *et al.* have employed atomic oxygen for growing NiO monolayer films on Ag(100), and have reported the formation of stoichiometric NiO(1×1) structures of a uniform monoatomic thickness.[10]

In this work, we have prepared highly ordered Ni-oxide nanostructures on Ag(100) by reactive evaporation of Ni in molecular oxygen and have characterized their atomic structure and morphology by high-resolution STM. By careful control of the experimental growth and postannealing parameters we are able to establish the appropriate conditions for the occurrence of the $p(2 \times 1)$ and (1×1) NiO structures. By stepwise increasing the annealing temperature we are able to trace the transformation from (i) a poorly ordered (2×1) phase after room-temperature deposition into (ii) a highly ordered (2×1) phase after annealing up to 400 K; (iii) a mixture of the (2×1) phase with emerging NiO(100)(1×1) islands between 400 and 500 K, and (iv) a single-phase NiO(100)(1×1) layer between 550 and 600 K; (v) finally, the so-called labyrinth phase consisting of high-aspect ratio, i.e., long and narrow, NiO(100)(1×1) island structures embedded into the Ag surface evolves after annealing to 700 K.

The evolution and the morphologies of the various surfaces have been analyzed by quantitative evaluation of high-resolution STM images in conjunction with model calculations by density-functional theory (DFT). The driving forces responsible for the metamorphosis of the Ni-oxide nanostructures on Ag(100) are investigated with the help of the DFT total-energy calculations. It is found that increasing the temperature leads to progressively more and more thermodynamically favored phases, from the initial kinetic product—the (2×1) precursor

phase—to NiO(100)(1 × 1) monolayer islands with bilayer insertions, to a final labyrinth phase.

II. EXPERIMENT AND THEORY

The experiments were carried out in a custom-designed multipurpose ultra-high-vacuum (UHV) system (base pressure $\sim 1 \times 10^{-10}$ mbar) equipped with an Omicron VT-STM, a low-energy electron diffraction (LEED) optics, and a cylindrical mirror analyzer for Auger electron spectroscopy as well as with facilities for sample cleaning and thin-film preparation. STM images were acquired at room temperature in constant current mode with electrochemically etched W tips; bias values are referred with respect to the sample; positive sample bias thus corresponds to the electrons tunneling into the empty states of the sample. The Ag(100) surface was cleaned by standard procedures, i.e., repeated cycles of Ar^+ ion sputtering (1 kV, 15 $\mu A/cm^2$) and annealing at 700 K; order and cleanliness of the substrate were checked by LEED, STM, and Auger electron spectroscopy.

The standard preparation procedure for NiO films in this work was by evaporation of Ni (using a commercial electron-beam evaporator) in an O_2 atmosphere of 1×10^{-6} mbar with the Ag surface at room temperature (RT). Some experiments were undertaken for evaporation conditions at elevated substrate temperatures as reported by Rota *et al.*[10] However, in these cases rough and less well-ordered films were obtained, which could not be analyzed with atomic precision in STM. For this reason we decided to concentrate on the standard RT deposition procedure in this work. Note that a significant role of the substrate temperature during deposition on the morphology and phase formation of oxide films has also been found in Refs. 11 and 12. The evaporation rate was measured with a quartz microbalance. The Ni-oxide coverage is defined by the evaporated amount of Ni in monolayers [ML, as referenced to the atom density of the Ag(100) surface], which for pseudomorphic growth corresponds to the NiO coverage. The deposited films were postannealed by heating in vacuum or in oxygen, at partial pressures between 1×10^{-6} and 1×10^{-7} mbar. Typically, the sample was kept at the respective annealing temperature for 10 min; in cases where an oxygen atmosphere was present the oxygen was pumped off after the sample had cooled down to below 400 K.

DFT calculations were performed using the QUANTUM ESPRESSO package,[13] employing a basis set of plane waves, ultrasoft pseudopotentials,[14] and the Perdew-Burke-Ernzerhof (PBE) exchange-correlation (xc) functional.[15] All the calculations were performed spin polarized by applying a pure DFT approach or a DFT + U approach;[16] in the latter case the value of U on the Ni atoms was chosen between 4.0 and 5.3 eV.[17] The first-neighbor distance in the metal support was set to 2.94 Å, corresponding to the equilibrium lattice parameter of bulk Ag according to our DFT approach, to be compared with an experimental value of 2.89 Å. The metal support was modeled by four Ag slabs in (100) stacking kept frozen in their bulk lattice positions, whereas the oxide monolayer was relaxed until the forces on the oxide atoms resulted in smaller than 0.01 eV/Å. Along the z axis, a minimum empty space of 15 Å was chosen to avoid interactions between replicated cells. A dipole correction[18] was applied to cancel spurious Coulombic interactions among replicated images. Values of 40 and 240 Ry were chosen as the energy cutoff for the selection of the plane waves for the description of the wave function and the electronic density, respectively. In the case of small unit cell (containing only four Ni and four O atoms) the first Brillouin zone was k sampled by employing a (4,4,1) grid, and the electronic levels were broadened with a Gaussian smearing of about 0.03 eV. STM images were simulated applying the Tersoff-Hamann approach[19] at a constant height of about 2 Å above the oxide surface (this small height value is justified by the low bias at which the STM images were recorded).

III. RESULTS

After reactive deposition of 2/3 ML of Ni onto the Ag(100) surface at room temperature, a (2 × 1) structure, the so-called precursor phase,[6] forms as evidenced by weak extra spots in LEED and the appearance of adjacent bright and dark rows in STM images (not shown). The surface displays small domains of only moderate order and two Ag height levels that are separated by a random pattern of step edges. The (2 × 1) structures are embedded into the Ag substrate rather than being accommodated on top of the silver surface. The Ni-oxide (2 × 1) coverage of the surface as evaluated from STM images is 0.62 ± 0.02, in good agreement with the nominal amount of deposited Ni.

Postannealing the Ni-oxide covered surface at 400 K (either in vacuum or in oxygen) gives rise to well-ordered, single-phase (2 × 1) structures embedded into the Ag substrate, as depicted in Fig. 1. Rectangular islands with straight boundaries as well as straight Ag step edges are observed [Fig. 1(a)]. However, a number of defects are also seen in the (2 × 1) areas, in particular, close to the phase boundaries, as indicated by the arrows in Fig. 1(a). A height histogram derived from the STM image, Fig. 1(b), is displayed in Fig. 1(c). The embedded patches of the precursor (2 × 1) phase are found both in the top layer (48% of total area) as well as in the bottom layer (13%).

Upon postannealing the as-deposited surface at 450 K in oxygen (1×10^{-7} mbar), the first islands of the NiO(100)(1 × 1) phase appear and a mixture of the (2 × 1) and the (1 × 1) phases is observed in Fig. 2. The high-resolution STM image of Fig. 2(a) shows a region of coexistence of the (2 × 1) phase with a NiO(1 × 1) island (B); several Ag islands (A) are also visible. Atomically resolved contrast is apparent on the NiO(1 × 1) island (B) as well as on the Ag islands (marked A). Typically, the (1 × 1) islands are found in the vicinity of antiphase domain boundaries of the (2 × 1) phase. Two types of antidomain boundaries can be discerned: the first type consists of domains rotated by 90° with respect to each other as seen in the upper part of Fig. 2(a); the second type consists of areas which are shifted by half a lattice spacing with respect to each other [see the middle part of Fig. 2(a)]. It appears that the antiphase domain boundaries act as nucleation centers for the NiO(1 × 1) islands, in particular, the boundaries separating (2 × 1) phases with perpendicular orientation. In the large-scale image of Fig. 2(b) the two different oxide phases (darker contrast) embedded in the Ag substrate (bright areas) are clearly discernible. Analysis of the height distribution in Fig. 2(b) reveals that the area covered by the two oxide phases

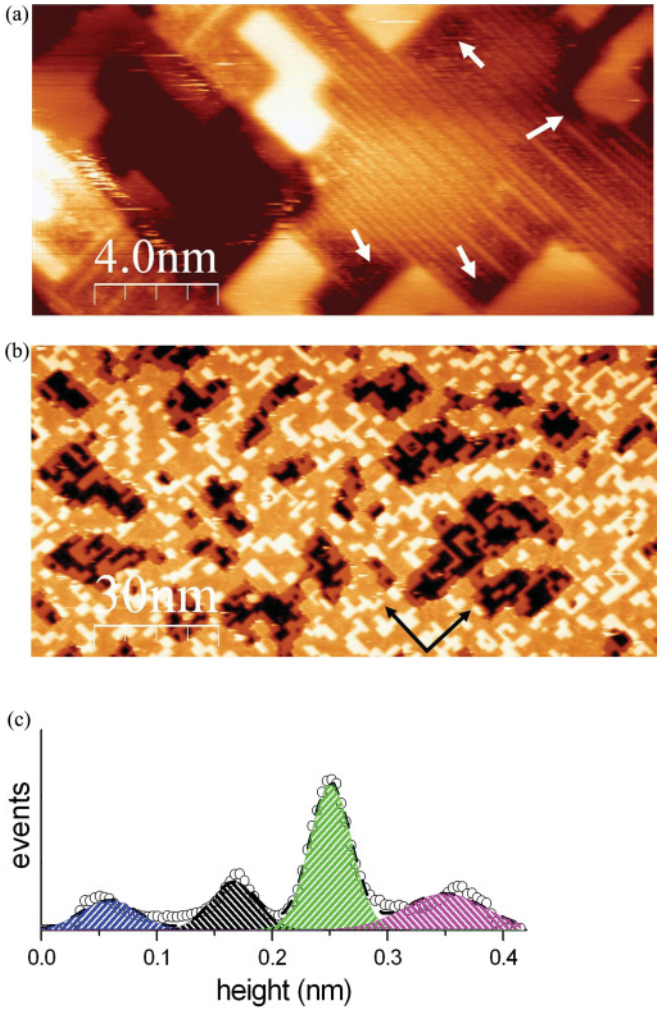

FIG. 1. (Color online) STM images of 2/3 ML of NiO on Ag after postannealing at 400 K in vacuum. (a) 20×10 nm^2, $U = -0.1$ V, $I_t = 0.2$ nA. The white arrows point at defects in the (2×1) phase. (b) 150×75 nm^2, single terrace, $U = -1$ V, $I_t = 0.1$ nA. The $\langle 110 \rangle$ directions are indicated by the black arrows. (c) Height histogram of panel (b) (open dots) fitted with four Gaussians (fit indicated by the dashed line). Peaks from left to right: Blue: NiO(2×1) precursor phase of bottom layer (dark areas in STM images; 13%); black: Ag of bottom layer [dark grey areas in panel b (red in color); 17%]; green: NiO (2×1) precursor phase of top layer [light grey areas in panel b (orange in color); 48%]; magenta: Ag of top layer (bright areas in STM images; 22%).

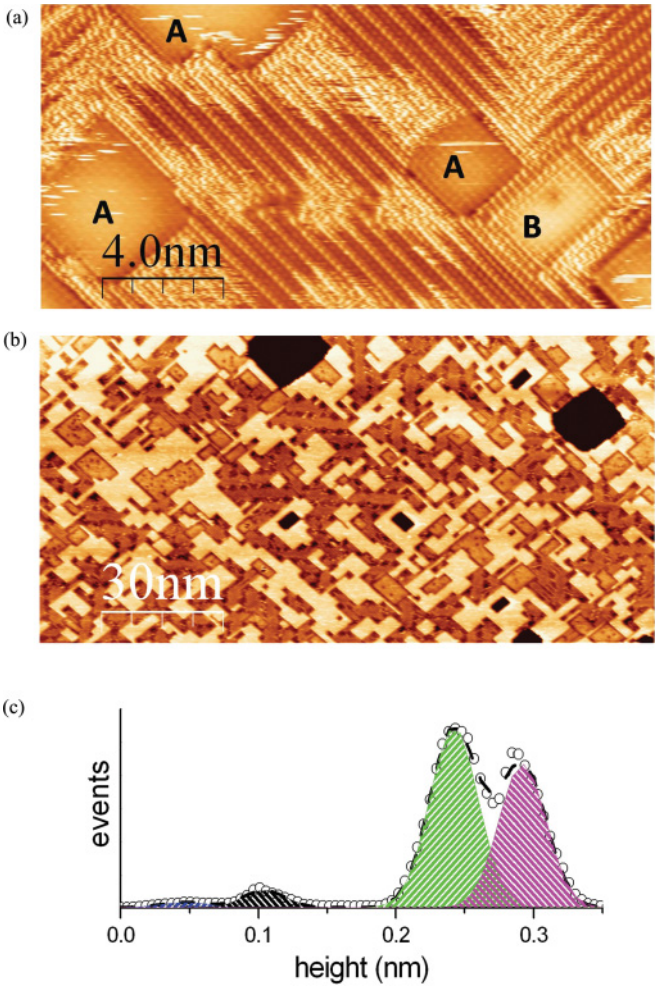

FIG. 2. (Color online) STM images of 2/3 ML NiO/Ag(100) postannealed at 450 K in oxygen ($p_{O_2} = 1 \times 10^{-7}$ mbar). (a) 20×10 nm^2, $U = -0.5$ V, $I_t = 0.9$ nA. Ag patches (A) and the NiO(1×1) island (B) are indicated. (b) 150×75 nm^2, single terrace, $U = 1$ V, $I_t = 0.4$ nA. (c) Height histogram for panel (b) (open dots) fitted with four Gaussians (fit indicated by the dashed line). Peaks from left to right: Blue: NiO(2×1) precursor phase of bottom layer (1%); black: Ag of bottom layer [dark holes in panel (b); 4%]; green: NiO(2×1) precursor phase of top layer plus emerging NiO (1×1) islands [light grey areas in panel b (orange in color); 45% (2×1) phase; 8% NiO (1×1) islands]; magenta: Ag of top layer [bright patches panel (b); 42%].

has shrunk to 53% as compared to 62% after deposition [see Fig. 2(c)]. As both oxide phases appear with a similar height contrast in the STM, the fraction of the NiO(1×1) phase with respect to the (2×1) phase has been determined to 0.18 by pixel counting. The difference of 9% between the as-deposited Ni-oxide coverage and the one measured here indicates that a fraction of Ni and O atoms has gone subsurface. Part of them may be incorporated as "defects" in the layer below the NiO (1×1) islands as suggested by the dark areas on the NiO(1×1) islands in Fig. 2(b).

After annealing to 600 K, the (2×1) phase has been completely replaced by NiO(1×1) islands, irrespective of whether the annealing has been performed in oxygen or in vacuum. A high-resolution STM image of a NiO(1×1) island embedded into the Ag substrate is shown in Fig. 3(a). The oxide island is distinguished by sharp and straight boundaries to the surrounding Ag substrate. A mosaic structure is seen on the atomically resolved contrast of the island surface. In the large-scale image displayed in Fig. 3(b), this mosaic structure gives the impression of a highly corrugated island surface. In Fig. 3(c), the height histogram of the image 3(b) is plotted. Interestingly, although large vacancy islands are found on this surface, the NiO islands are exclusively found embedded in the upper level Ag layer. The area covered by the NiO(1×1) phase is now only 0.34 ± 0.02 according to the height distribution analysis, suggesting the formation of partly second-layer NiO islands (see below). A line scan across a vacancy Ag island

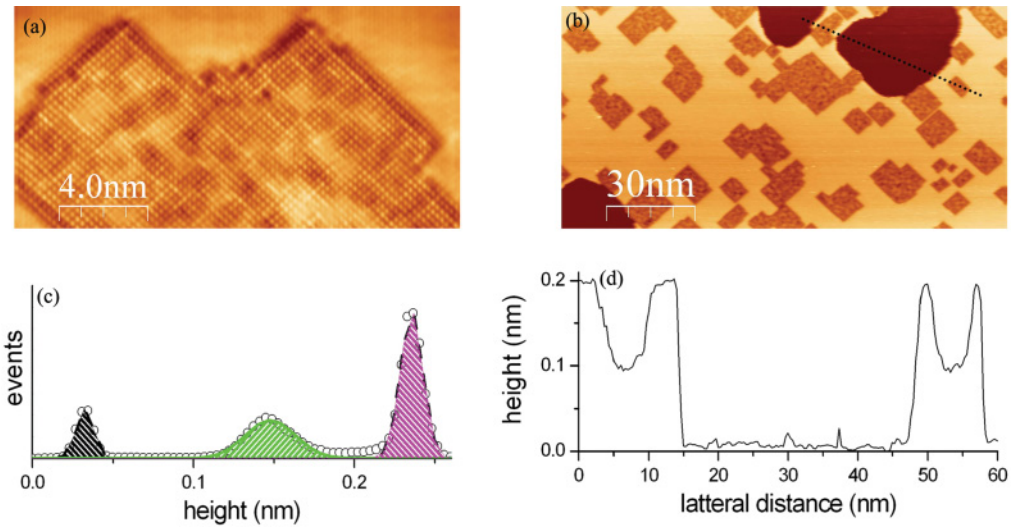

FIG. 3. (Color online) STM images of 2/3 ML NiO/Ag(100) postannealed at 600 K in oxygen ($p_{O_2} = 1 \times 10^{-7}$ mbar). (a) 20×10 nm^2, $U = -0.85$ V, $I_t = 0.5$ nA, Fourier filtered. (b) 150×75 nm^2, $U = -1$ V, $I_t = 0.1$ nA. The dotted line indicates the direction of the line scan in panel (d). (c) Height histogram of panel (b) (open dots) fitted with three Gaussians (fit indicated by the dashed line). Peaks from left to right: Black: Ag of bottom layer (dark areas in panel b; 13%); green: NiO (1×1) islands (34%); magenta: Ag of top layer (bright area in STM images; 43%). (d) Line scan across the Ag vacancy island along the dotted line in (b), with two small NiO(1×1) islands adjacent to it.

with two small NiO(1×1) islands adjacent to it is depicted in Fig. 3(d).

Increasing the annealing temperature to around 650 K, the rectangular and square embedded NiO (1×1) islands transform into small, high-aspect ratio NiO(1×1) structures separated by thin Ag "walls," [see Figs. 4(a) and 4(b)]. The STM pattern looks like an airborne street map of a city, and for convenience is termed "labyrinth" morphology. In Fig. 4(c), the surface as obtained by annealing at 680 K in oxygen (1×10^{-7} mbar) is almost completely covered by the labyrinth structures; only a few larger square or rectangular NiO(1×1) and Ag islands are seen. Figure 4(d) is a height histogram derived from the STM image, Fig. 4(c). The histogram analysis indicates that the overall area covered by the NiO(1×1) phase has recovered to 0.53, with 0.11 of it with darker STM contrast.

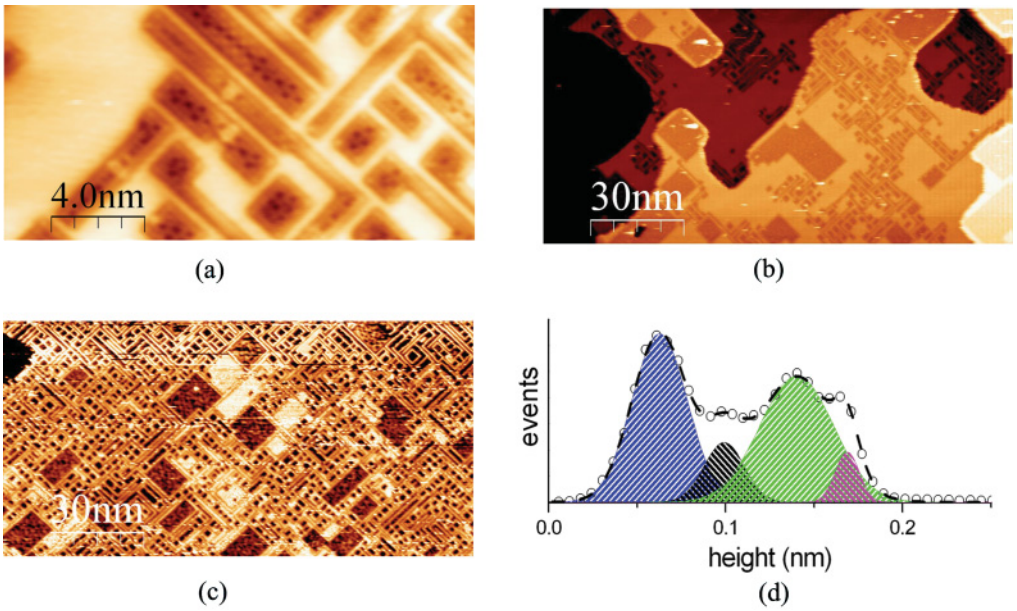

FIG. 4. (Color online) STM images of 2/3 ML NiO/Ag(100) after postannealing at 650–680 K in vacuum. (a) 20×10 nm^2, $U = -2$ V, $I_t = 0.8$ nA. (b) 150×75 nm^2, $U = -2$ V, $I_t = 0.1$ nA. (c) 150×75 nm^2, $U = 1.4$ V, $I_t = 0.8$ nA. (d) Height histogram of panel (c) (open dots) fitted with four Gaussians (fit indicated by the dashed line). Peaks from left to right: Blue: NiO(1×1) labyrinth islands (42%); black: larger NiO(1×1) islands (11%); green: Ag (42%); magenta: distorted Ag areas (5%).

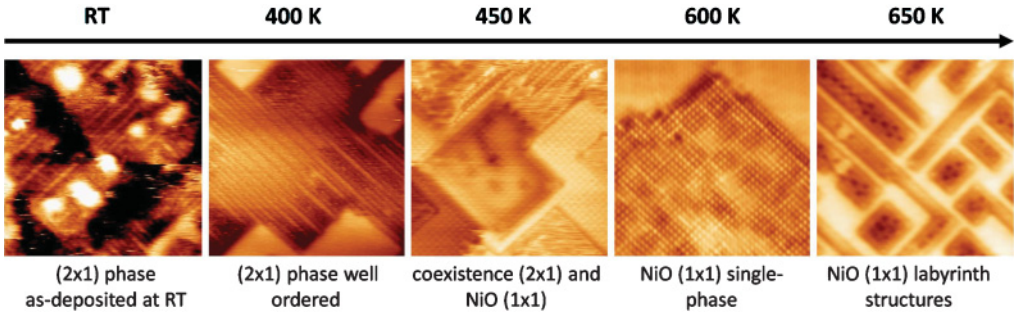

FIG. 5. (Color online) Evolution of the morphology of 2/3 ML NiO/Ag(100) as a function of temperature. (STM images: 10×10 nm^2; RT image: $U = -0.2$ V, $I_t = 0.8$ nA; other images taken from Figs. 1, 2, 4, and 5).

IV. DISCUSSION

The evolution of the morphology of the 2/3 ML NiO-covered Ag(100) surface as a function of temperature is summarized in Fig. 5. The surface after reactive deposition of Ni at room temperature is rough on a two-Ag-level scale, displaying a top Ag layer with small areas of embedded NiO(2×1) structures and interrupted by Ag vacancy islands of monoatomic depth. The latter are randomly distributed, and display irregular boundary lines (step edges) and an average characteristic size parameter of about 11 nm. Annealing to 400 K significantly improves the surface order, rectangular NiO(2×1) and Ag domains develop with straight domain boundaries and straight step edges; the Ag vacancy islands also change shape into rectangular structures. Annealing temperatures exceeding 400 K (∼420–450 K) induce the transformation from the (2×1) precursor phase to the pseudomorphic NiO(1×1) phase. The NiO(1×1) islands are found next to Ag patches with most of the islands almost entirely enclosed by the Ag substrate. The (2×1) and (1×1) phases coexist for a temperature range of about 150 K in well-defined geometric structures, but the equilibrium between the two phases gradually shifts toward the (1×1) phase until at 600 K, the (1×1) structure exists as single phase in islands embedded into the Ag substrate. Annealing to higher temperatures leads to the disintegration of the large (1×1) islands into narrow, high-aspect ratio (1×1) islands forming the so-called labyrinth morphology. The characteristic labyrinth island size decreases with temperature reaching a value of ∼2–3 nm after 680 K annealing. It is noted that the oxygen pressure during the heating steps appears to play only a minor role for this evolution of morphology: annealing in oxygen or in vacuum produced similar results, suggesting that thermodynamic forces are at play in these phase transformations. The NiO/Ag surfaces are stable in vacuum for days; small effects of reduction by reaction with residual gases could be reverted by brief annealing in oxygen at the respective temperatures.

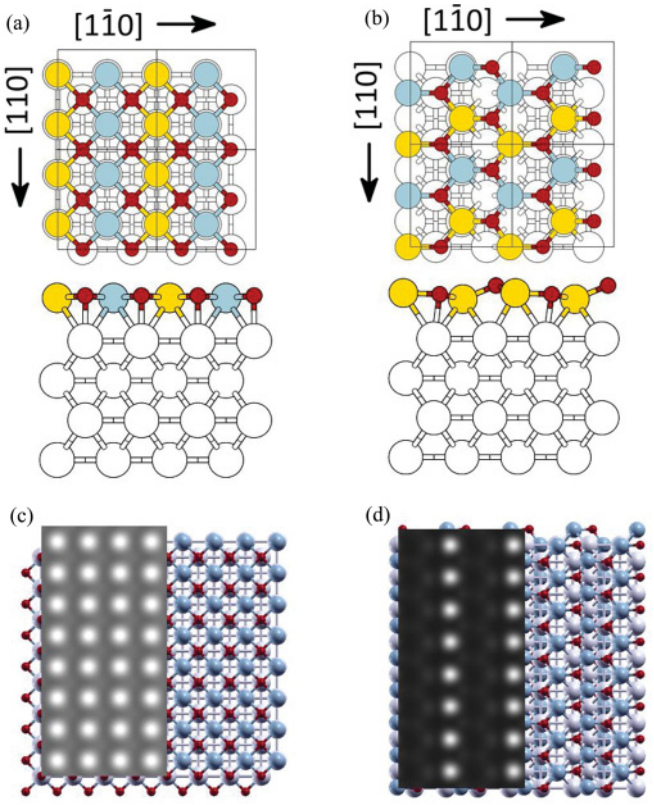

FIG. 6. (Color online) Structural models [(a) and (b)] and simulated STM images at positive bias [(c) and (d)] as derived from DFT of the NiO(100)(1×1) [(a) and (c)] and the (2×1) precursor phase [(b) and (d)]; top views (top panels) and side views (bottom panels). White: Ag; dark and light grey (blue and yellow in color): Ni (spin up and spin down, respectively); black (red in color): O atoms. The ⟨110⟩ directions are indicated by the black arrows.

The structure of the NiO(100)(1×1) phase—shown in Fig. 6(a)—is homologous to that of similar oxides exhibiting rocksalt crystal structure in the bulk, which easily grow with (100)/(100) epitaxy on Ag(100). A possible structural model of the (2×1) phase—shown in Fig. 6(b)—was previously suggested in Ref. 9. It consists of a Ni layer and an O layer with distorted hexagonal structure, reminiscent of the NiO(111) stacking. This structure has been validated by the present DFT calculations, as we find that it represents a local minimum and is robust with respect to moderate annealing (300 K) via Car-Parrinello simulations. It can be noted that two types of oxygen and nickel atoms are present in the (2×1) phase, as belonging to ridges or valleys running along ⟨110⟩ directions. From the simulated STM images of Fig. 6, it should also be emphasized that the contrast is reversed in the (1×1) and (2×1) phases: in the former, Ni atoms are imaged as bright spots, whereas in the latter the O atoms of the ridges appear as protrusions. This difference is connected with the different topography of the two phases, with the (2×1) structure being

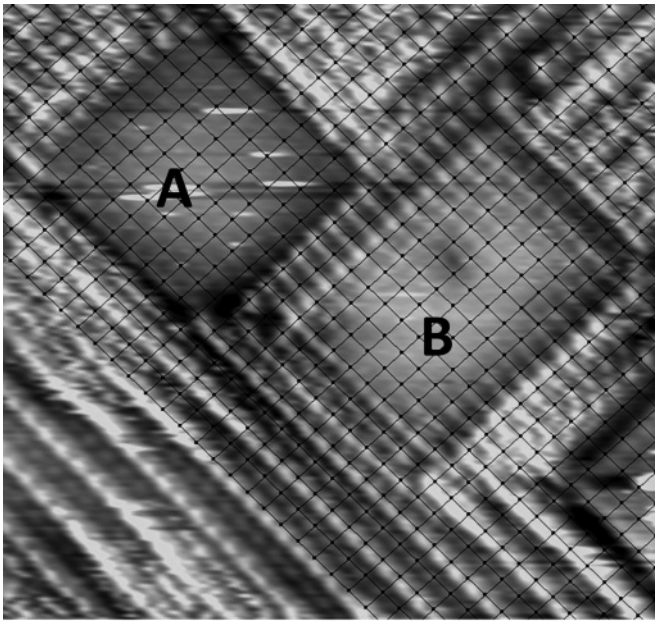

FIG. 7. STM image of an Ag island (A) and a NiO(1 × 1) island (B) (7.8 × 7.4 nm^2, $U = -0.5$ V, $I_t = 0.9$ nA). The grid superimposed on the protrusions of the Ag island is in registry with the protrusions on the NiO island.

a polar phase [in contrast with the practically flat (1 × 1) phase], thus similar to other polar stoichiometric phases such as CoO/Pd(100).[20] This is confirmed by the atomically resolved STM images in Fig. 7, allowing us to substantiate the atomic species that are imaged as protrusions in the STM. In Fig. 7, a grid is drawn on top of the maxima of the NiO(1 × 1) island (marked B), which extends also over the neighboring Ag island (A): it is clearly apparent that the maxima in both islands are located at the crossings of the grid. Since the NiO island is embedded into the Ag surface layer, there is a shift of one half unit-cell vector between the second Ag layer, on which the NiO island sits, and the top Ag layer. From the theoretical model of the NiO(1 × 1) overlayer presented in Fig. 6(a), it is predicted that the Ni atoms are located in the fourfold hollow sites of the Ag(100), and thus that the Ni atoms of the (1 × 1) phase are imaged as maxima in the STM at the given tunneling conditions; experiment and theory are thus in agreement.

Table I reports the relative energetics of the two phases evaluated via DFT + U fully relaxed geometry optimizations as a function of the U value and the spin state. For the (1 × 1) phase, the ferromagnetic state (FM) is compared with an antiferromagnetic state (AFM2) in which parallel spins are

TABLE I. Relative energetics of the (1 × 1) and (2 × 1) NiO phases on Ag(100) as a function of the U value on Ni atoms and for several magnetic orderings (see text for more details).

U	(1 × 1) phase		(2 × 1) phase		
(eV)	AFM2	FM	AFM3	AFM2	FM
0.0	+0.16	+0.22	+0.02		+0.00
4.0	+0.00	+0.07	+0.32	+0.39	+0.38
5.3	+0.00	+0.05	+0.37		+0.46

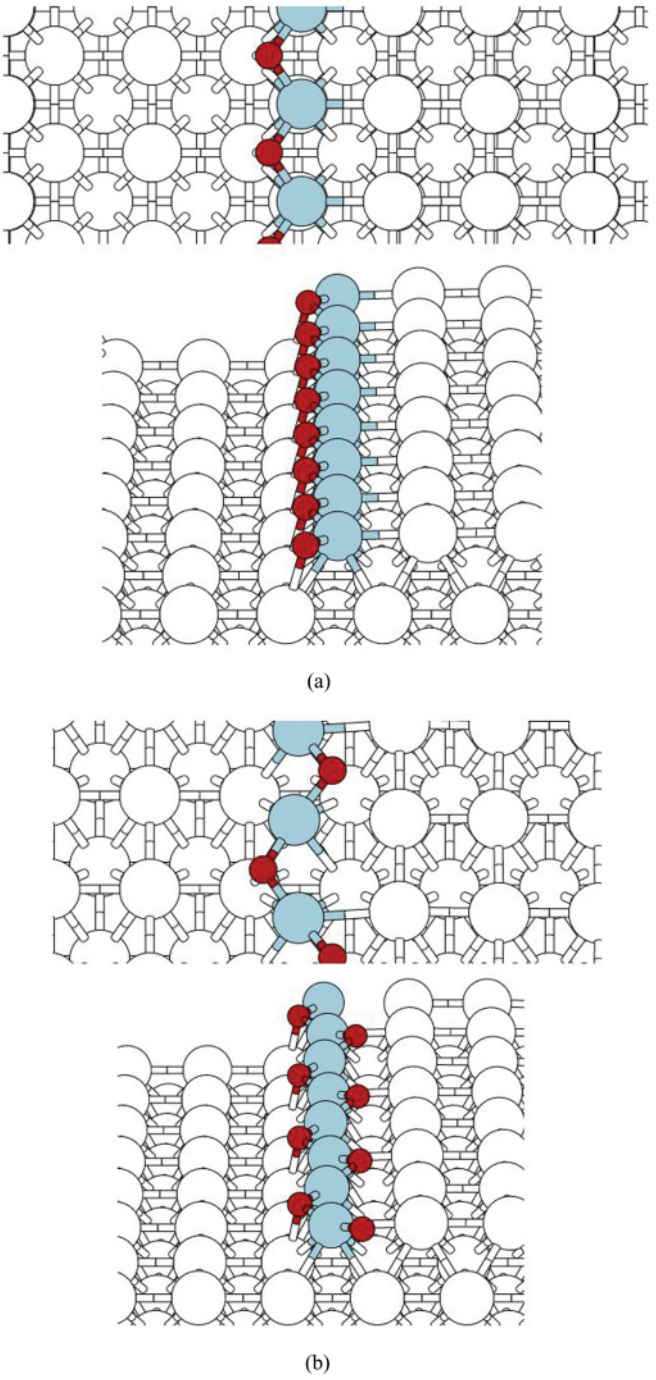

FIG. 8. (Color online) Structural models of the early stages of growth of a NiO monolayer on Ag(100). (a) Single NiO row grown according to a (1 × 1) pattern or (b) according to a (2 × 1) pattern. White: Ag; dark grey (blue in color): Ni; black (red in color): O atoms.

arranged along ⟨110⟩ lines (see also the color coding in Fig. 6). For the (2 × 1) phase, in addition to the FM and AFM2 states, a further antiferromagnetic configuration (AFM3) is reported in which parallel spins are arranged in a zigzag fashion running along a ⟨110⟩ direction. Interestingly enough, the energy order of the two phases and also of the spin configurations is inverted by varying U, switching from (2 × 1) FM < (2 × 1) AFM3 < (1 × 1) AFM2 < (1 × 1) FM for $U = 0$, to (1 × 1) AFM2 <

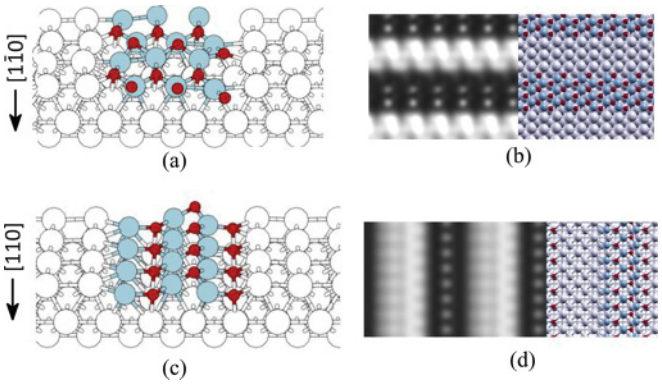

FIG. 9. (Color online) Structural models and DFT-simulated STM images of the borders between the embedded precursor (2×1) phase of NiO and the Ag(100) surface; [(a) and (b)] [1$\bar{1}$0] border and [(c) and (d)] [110] border. The directions of the borders are indicated by the black arrows. White: Ag; dark grey (blue in color): Ni; black (red in color): O atoms.

(1×1) FM $<$ (2×1) AFM3 $<$ (2×1) FM for $U = 4.0$–5.3 eV. Only the latter results are in tune with experiment, which points to the (1×1) phase as the thermodynamically stable one, thus confirming the need of including a $U > 0$ term into the DFT Hamiltonian for a proper description of NiO nanostructures.[17] All the DFT values to be discussed in the following have thus been obtained using $U = 4$ eV.[17]

The reason why the (2×1) phase is initially formed must therefore be of kinetic origin. A model for the early stages of growth of a NiO wire on a step edge of Ag(100) is shown in Fig. 8. The energy difference between (2×1) and (1×1) nucleation shown in this figure is about 0.4 eV per NiO unit, thus proving that the formation of the (1×1) wire is strongly disfavored with respect to the (2×1) one. Furthermore, when growing according to the (2×1) arrangement, the (2×1) precursor phase prefers to be embedded into the Ag surface by 0.18 eV per NiO unit with respect to the "on-top" growth, in agreement with experimental observations. When growing along the step edge of the Ag(100) surface, the (2×1) phase prefers to expose a [1$\bar{1}$0] border [i.e., the rows of the (2×1) phase are oriented perpendicular to the step edge; see Fig. 9(a)] rather than a [110] border [i.e., the rows of the (2×1) phase are oriented parallel to the step edge; see Figs. 9(c) and 9(d)], higher in energy by 0.19 eV per NiO unit. The [1$\bar{1}$0] border is structurally much more flexible than the [110] one, and induces a noticeable reconstruction in the nearby metal structure, determining an irregular STM pattern [see Fig. 9(b)], which turns out to be similar to that of the defects highlighted in Fig. 1(a) in the proximity of the metal/oxide borderline. The defects in the (2×1) phase visible in Fig. 1(a) can thus be interpreted as nucleation regions of the (2×1) precursor phase at extended steps of the Ag(100) surface. The [110] border, although energetically disfavored, must nevertheless be formed for simple geometrical reasons when the embedded precursor phase grows along the [110] direction.

The embedded (1×1) monolayer is thermodynamically favored with respect to the embedded (2×1) monolayer. The formation of this phase is also favored with respect to the formation of an embedded (1×1) bilayer: transforming a one monolayer stripe $2N$ Ni-atom wide into a bilayer stripe N Ni-atom wide costs about $N \times 0.05$ eV. However, the monolayer system is not in perfect epitaxial lattice match with the support, but is slightly strained. As discussed in Ref. 17, it is possible to predict the optimal lattice parameter of an ultrathin oxide film by minimizing its effective energy, defined as the sum of the energy of a freestanding oxide slab plus the oxide/support adhesion energy. Our DFT calculations predict the following equilibrium values: 2.87 Å for 1 ML (1×1), 2.93 Å for BL (1×1), and 2.98 Å for bulk NiO, 2.94 Å for bulk Ag (where ML = monolayer and BL = bilayer). A (1×1) ML NiO is thus slightly strained on Ag(100), whereas a (1×1) BL is practically in match with the Ag support. The value of the ML stickiness,[17] i.e., the second derivative of the effective oxide energy with respect to the lattice parameter, however, is 21.18 eV Å^{-2} at the DFT level, and is not negligible. An efficient way to release this strain is to insert occasional BL patches underneath the ML structure, as this increases the optimal lattice parameter of the resulting composite system, a compromise obtained at some cost (as discussed above, a BL is at higher energy than a ML). This is the origin of the dark-contrast defects in Fig. 3(a), and explains the reduction of about 30% in the NiO area.

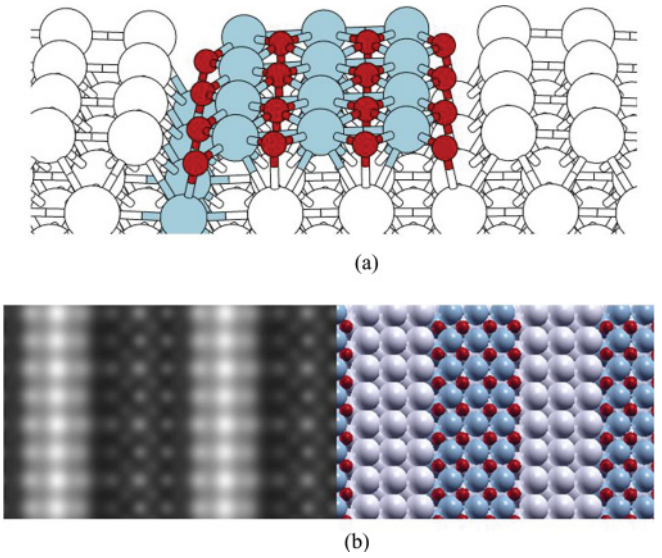

FIG. 10. (Color online) Structural models [(a) and (b)] and simulated STM image (b) of a labyrinth phase, in which a monoatomic row of NiO can be observed at the border with silver underneath the surface NiO monolayer. White: Ag; dark grey (blue in color): Ni; black (red in color): O atoms.

An alternative mechanism of strain relaxation is shown in Fig. 10: in this case we consider a very narrow NiO(1×1) stripe (only three Ni-atom wide) intercalated with thin Ag walls (3 Ag-atom wide), resembling the structure of the labyrinth phase stabilized at high temperature as shown in Fig. 4. We found that a (1×1) stripe can be strongly stabilized by inserting a Ni row into the second (subsurface) layer in such a way that a NiO bilayer line forms at the boundary of the island (see Fig. 10). This decreases the energy of the system by 0.08 eV per NiO unit with respect to a perfect ML stripe. This configuration is also more stable than the on-top growth of an extended (1×1) ML, and is thus predicted to be the thermodynamically stable configuration of a NiO at

sub-ML coverage, in excellent agreement with the formation of the labyrinth phase at high temperature. The presence of a subsurface Ni row darkens the boundaries of the (1×1) stripes (see Fig. 10), again in good agreement with the darker rims visible in the experimental STM images of Figs. 3 and 4.

V. CONCLUSIONS

In summary, we have shown that the morphological evolution observed experimentally for NiO submonolayer deposits on Ag(100) as a function of temperature is fully rationalized by DFT + U calculations, and is the following. The (2×1) precursor phase is thermodynamically less stable than the (1×1) phase, but is kinetically favored due to the better adhesion to a Ag(100) step edge in the early stages of growth. Both phases are more stable when embedded into the Ag support. By increasing the temperature, mass transport phenomena start to take place. First, the (2×1) phase transforms into a (1×1) monolayer (which is more stable than a bilayer). The monolayer system is, however, slightly strained due to the lattice mismatch with respect to the substrate. This strain is initially released by inserting bilayer patches underneath the monolayer phase [appearing as dark-contrast defects in Fig. 3(a)]. At still higher temperatures, allowing a more substantial mass transport, this mosaic arrangement is then replaced by a labyrinth phase, in which narrow (1×1) monolayer stripes with $\langle 110 \rangle$ Ni borders decorated by second-layer monoatomic NiO wires are embedded into the Ag support. The NiO coverage area, which had appreciably decreased in the monolayer-with-underlying-bilayer-defects system, now increases back to values closer to the original one. It can be noted that no change in the stoichiometry of the system occurs in all these transformations, in agreement with experimental observation that the oxygen pressure plays a minor role in this system.

ACKNOWLEDGMENTS

This work has been supported by the ERC Advanced Grant SEPON. CPU time was provided by CINECA supercomputing center via the UT-Ox project.

*Present address: Physik Department E20, Technische Universität München, James-Franck Str. 1, D-85748 Garching, Germany.

[1] J. Wu, J. Choi, A. Scholl, A. Doran, E. Arenholz, Y. Z. Wu, C. Won, C. Hwang, and Z. Q. Qiu, Phys. Rev. B **80**, 012409 (2009).

[2] S. Altieri, L. H. Tjeng, and G. A. Sawatzky, Thin Solid Films **400**, 9 (2001).

[3] S. Altieri, L. H. Tjeng, F. C. Voogt, T. Hibma, O. Rogojanu, and G. A. Sawatzky, Phys. Rev. B **66**, 155432 (2002).

[4] A. M. Ferrari, S. Casassa, C. Pisani, S. Altieri, A. Rota, and S. Valeri, Surf. Sci. **588**, 160 (2005).

[5] A. M. Ferrari, S. Casassa, and C. Pisani, Phys. Rev. B **71**, 155404 (2005).

[6] I. Sebastian, T. Bertrams, K. Meinel, and H. Neddermeyer, Faraday Discuss. **114**, 129 (1999).

[7] M. Caffio, A. Atrei, B. Cortigiani, and G. Rovida, J. Phys.: Condens. Matter **18**, 2379 (2006).

[8] S. Großer, C. Hagendorf, H. Neddermeyer, and W. Widdra, Surf. Interface Anal. **40**, 1741 (2008).

[9] M. Caffio, B. Cortigiani, G. Rovida, A. Atrei, and C. Giovanardi, J. Phys. Chem. B **108**, 9919 (2004).

[10] A. Rota, S. Altieri, and S. Valeri, Phys. Rev. B **79**, 161401(R) (2009).

[11] Ch. Hagendorf, R. Shantyr, H. Neddermeyer, and W. Widdra, Phys. Chem. Chem. Phys. **8**, 1575 (2006).

[12] R. Shantyr, Ch. Hagendorf, and H. Neddermeyer, Thin Solid Films **464–465**, 65 (2004).

[13] P. Giannozzi, S. Baroni, N. Bonini, M. Calandra, R. Car, C. Cavazzoni, D. Ceresoli, G. Chiarotti, M. Cococcioni, I. Dabo, A. Dal Corso, S. De Gironcoli, S. Fabris, G. Fratesi, R. Gebauer, U. Gerstmann, C. Gougoussis, A. Kokalj, M. Lazzeri, L. Martin-Samos, N. Marzari, F. Mauri, R. Mazzarello, S. Paolini, A. Pasquarello, L. Paulatto, C. Sbraccia, S. Scandolo, G. Sclauzero, A. P. Seitsonen, A. Smogunov, P. Umari, and R. M. Wentzcovitch, J. Phys.: Condens. Matter **21**, 395502 (2009).

[14] D. Vanderbilt, Phys. Rev. B **41**, 7892 (1990).

[15] J. P. Perdew, K. Burke, and M. Ernzerhof, Phys. Rev. Lett. **77**, 3865 (1996).

[16] V. I. Anisimov, J. Zaanen, and O. K. Andersen, Phys. Rev. B **44**, 943 (1991).

[17] G. Barcaro, I. O. Thomas, and A. Fortunelli, J. Chem. Phys. **132**, 124703 (2010).

[18] L. Bengtsson, Phys. Rev. B **59**, 12301 (1999).

[19] J. Tersoff and D. R. Hamann, Phys. Rev. B **31**, 805 (1985).

[20] L. Gragnagniello, G. Barcaro, L. Sementa, F. Allegretti, G. Parteder, S. Surnev, W. Steurer, A. Fortunelli, and F. P. Netzer, J. Chem. Phys. **134**, 184706 (2011).